Vol. 491: 47–65, 2013
doi: 10.3354/meps10453

MARINE ECOLOGY PROGRESS SERIES
Mar Ecol Prog Ser

Published October 2

Contributions of mesozooplankton to vertical carbon export in a coastal upwelling system

Michael R. Stukel[1,3,*], Mark D. Ohman[1], Claudia R. Benitez-Nelson[2], Michael R. Landry[1]

[1]Scripps Institution of Oceanography, University of California at San Diego, La Jolla, California 92093, USA

[2]Marine Science Program and Department of Earth & Ocean Sciences, University of South Carolina, Columbia, South Carolina 29208, USA

[3]*Present address:* Horn Point Laboratory, University of Maryland Center for Environmental Science, Cambridge, Maryland 21613, USA

ABSTRACT: Mesozooplankton can directly impact global biogeochemical cycles by repackaging particulate organic carbon (POC) into dense, rapidly sinking fecal pellets and by undertaking vertical migrations that transport carbon and nutrients to depth. We assessed these contributions of mesozooplankton to vertical flux in the California Current Ecosystem, a productive but spatiotemporally variable coastal upwelling system, during cruises in April 2007 and October 2008. Sediment traps and Thorium-234 (^{234}Th) disequilibrium measurements were used to assess the total passive flux of sinking POC, while pigment analyses and microscopic enumeration of sediment trap samples provided estimates of total fecal carbon transport. Identification of mesozooplankton in paired day-night, vertically stratified plankton tows allowed calculation of the active transport of carbon by the dominant taxa of vertically migrating mesozooplankton (particularly copepods and euphausiids). Across the range of 9 ecosystem conditions encountered on the cruises, recognizable fecal pellet mass flux varied from 3.5 to 135 mg C m^{-2} d^{-1} (3 to 94% of total passive flux) at the 100 m depth horizon. The active transport of carbon by migratory mesozooplankton taxa contributed an additional 2.4 to 47.1 mg C m^{-2} d^{-1} (1.9 to 40.5% of total passive flux). Inter-cruise comparisons suggest that fecal pellets contributed a higher portion of passive export during the productive spring cruise, when fecal material may have been responsible for close to 100% of sinking material. During the fall cruise, a gradient was observed with carbon export in productive water parcels driven by a large contribution of fecal pellets. In the less productive regions, fall vertical fluxes contained a higher proportion of marine snow and unidentifiable particles.

KEY WORDS: Carbon flux · Sedimentation · Fecal pellet · Diel vertical migration · Copepod · Euphausiid · Export production · Detritus

INTRODUCTION

The 'biological pump', a critical component of global biogeochemical cycles, is responsible for transporting the carbon and nitrogen fixed by phytoplankton in the euphotic zone to the deep ocean (Ducklow et al. 2001). Within the biological pump, the relative contributions of phytoplankton production, aggregation (Alldredge & Gotschalk 1989, Jackson et al. 2005), mineral ballasting (Armstrong et al. 2001), and mesozooplankton grazing (Buitenhuis et al. 2006) to vertical carbon flux are still hotly debated and likely to vary spatially and temporally (Burd et al. 2010). While solid arguments exist supporting the importance of each export mechanism, the difficulty of quantifying and comparing individual processes *in*

*Email: mstukel@umces.edu

situ has resulted in investigators using a variety of models, which may support one hypothesis but not exclude others. As such, experimental evidence is needed to assess the nature of sinking material, and how it varies among and within ecosystems.

Mesozooplankton can mediate biogeochemically-relevant processes in many ways, and thus play crucial roles in global carbon and nitrogen cycles. By packaging organic matter into dense, rapidly sinking fecal pellets, mesozooplankton can efficiently transport carbon and associated nutrients out of the surface ocean on passively sinking particles (Turner 2002). In the California Current Ecosystem (CCE), for example, Stukel et al. (2011) have suggested that fecal pellet production by mesozooplankton is sufficient to account for all of the observed variability in vertical carbon fluxes. Diel vertically migrating (DVM) mesozooplankton may also actively transport carbon and nitrogen to depth when they feed at the surface at night but descend during the day to respire, excrete, and sometimes die (Longhurst et al. 1990, Steinberg et al. 2000, Al-Mutairi & Landry 2001). At times, mesozooplankton are also able to regulate carbon export rates by exerting top-down grazing pressure on phytoplankton (Goericke 2002, Olli et al. 2007, Landry et al. 2009) or consuming sinking particles (Wilson et al. 2010).

In this study, we utilize sediment traps and ^{234}Th:^{238}U disequilibrium to determine total passive sinking flux, and paired day-night vertically-stratified net tows to quantify the contributions of mesozooplankton to active transport during 2 cruises of the CCE Long-Term Ecological Research (LTER) program in April 2007 and October 2008. Using microscopic enumeration of fecal pellets we show that, across a wide range of environmental conditions, identifiable fecal pellets account for a mean of 35% of passive carbon export at 100 m depth, with pigment analyses suggesting that total sinking flux of fecal material may be even higher. On average, mesozooplankton active transport contributes an additional 19 mg C m^{-2} d^{-1} (1.9 to 40.5% of total passive flux at the base of the euphotic zone) that is not assessed by typical carbon export measurements.

MATERIALS AND METHODS

Cruises and sampling plans

Data for this study come from 2 cruises of the CCE-LTER program conducted during April 2007 (CCE-P0704) and October 2008 (CCE-P0810). During the study, water parcels with homogeneous characteristics were identified using satellite images of sea surface temperature and chlorophyll and site surveys with a Moving Vessel Profiler (Ohman et al. 2012). Appropriate patches for process experiments were marked with a surface drifter with holey sock drogue at 15 m (cf. Sybrandy & Niiler 1992; see Fig. 1) and tracked in real time using Globalstar telemetry. Another similarly drogued drift array with attached sediment traps (at 1 or 2 depths) was also deployed in close proximity to collect sinking particulate matter over the 2 to 4 d duration of each experimental cycle. During each experiment, paired day-night depth-stratified samples of mesozooplankton were taken with a 1 m^2, 202 µm mesh Multiple Opening and Closing Net and Environmental Sensing System (MOCNESS) at 9 depths over the upper 450 m of the water column, with the midpoint of the tow corresponding approximately to the location of the surface drifter. These samples were later enumerated by ZooScan (as described below) and grouped into broad taxonomic categories and size classes for calculation of mesozooplankton active transport. Oblique bongo tows (0.71 m diameter, 202 µm mesh) to 210 m were also taken at mid-night and mid-day to collect organisms for determination of size-fractionated dry weights and grazing rates of the mesozooplankton community. Size-fractionated dry weights were converted to carbon biomass using the dry weight to carbon relationships of Landry et al. (2001).

^{234}Th export measurements

^{234}Th deficiencies of the water parcels were determined from 4-l samples taken at 8 to 10 depths per cast of a CTD Niskin rosette, following established small-volume procedures (Benitez-Nelson et al. 2001b, Buesseler et al. 2001, Pike et al. 2005). Immediately after collection, samples were acidified to a pH of ~2 with concentrated HNO_3 and spiked with ^{230}Th (1 ml at 10 dpm ml^{-1}). Four hours later, NH_4OH was added to adjust to a pH of ~9, and 100 µl each of $KMnO_4$ (7.5 g l^{-1}) and $MnCl_2$ (33 g l^{-1}) were added. Samples were shaken and allowed to equilibrate for >8 h as the Th co-precipitated with MnO_2. Precipitates were vacuum filtered under high-pressure onto 25 mm quartz microfiber (QMA) filters and mounted into RISO sample holders. Samples were counted ashore with a low-level RISO beta counter at the University of South Carolina. After >6 half-lives had passed, they were again counted to establish background beta emission levels. Filtration yields were

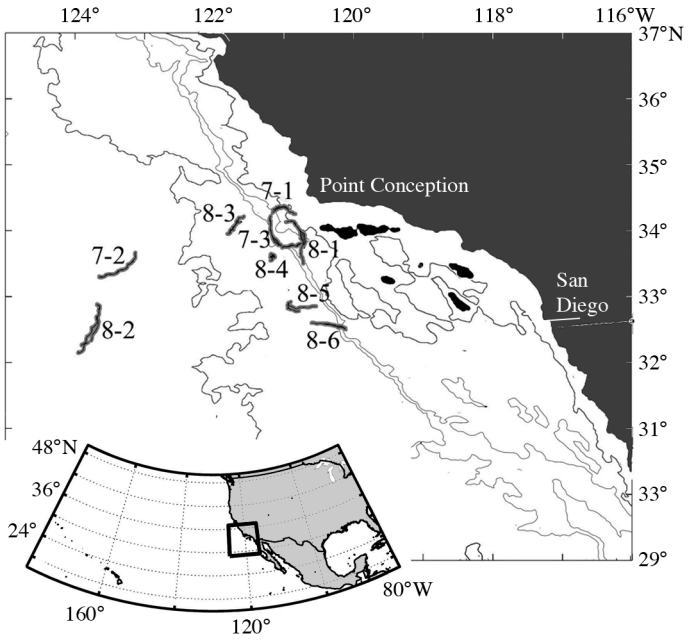

Fig. 1. Bathymetric map of study region off Point Conception, California. Thin gray lines are depth contours of 1000, 2000, 3000, and 4000 m. Black lines upon a gray background are drifter tracks. Numbers indicate drifter tracks for the cycles from cruises P0704 and P0810 (e.g. 8-1 is P0810, Cycle 1). Inset map shows our study region (thick black box) in the western North Pacific

calculated by Inductively Coupled Plasma Mass Spectrometry at the Woods Hole Oceanographic Institution Analytical Facility after addition of a gravimetrically measured aliquot of ^{229}Th (99.5 dpm) and column chromatography in AG1-X8 100-200 mesh chloride form resin to purify the Th isotopes. Recoveries averaged 86%. ^{238}U was assumed to covary with salinity and calculated from the equation: ^{238}U (dpm l^{-1}) = 0.0786 × salinity – 0.315 (Owens et al. 2011). Deficiency was calculated as the difference between ^{238}U and ^{234}Th. ^{234}Th export was determined using a 1-dimensional steady-state model [$E = \lambda_{Th} (A_U - A_{Th})$] and trapezoidal vertical integration. Although this steady-state model oversimplifies the complex processes affecting particulate and dissolved Th cycling in the ocean euphotic zone, it closely matched the ^{234}Th fluxes in sediment traps for 8 out of the 9 cycles assessed (see Fig. 2).

^{234}Th export was converted to vertical carbon flux by multiplying by experimentally determined C:^{234}Th ratios. Particulate samples for the determination of the C:^{234}Th ratio were collected using 2 independent methods: sediment traps and *in situ* pumps. Samples were routinely collected at a depth horizon of 100 m, and they were also collected from a depth just below the base of the euphotic zone (50 to 60 m) on the P0810 cruise. Sediment trap C:Th samples were collected as discussed below. *In situ* pump samples were collected using a McLane WTS-LV pump with pre-filters to size-fractionate the collected particles. On the P0704 cruise, >20 µm particles were used to calculate the C:^{234}Th ratios. On the P0810 cruise, we used >50 µm particles for these calculations (comparison of the ratios of contemporaneous pump and sediment trap C:^{234}Th samples showed no significant difference between samples collected on 20 and 50 µm mesh; $p > 0.3$ with a Kolmogorov-Smirnov test). In each case, 300-l samples of seawater were filtered through a Nitex filter, which was then rinsed onto a 25 mm QMA filter. QMA filters for the C:^{234}Th ratio were counted on land similarly to the water-column ^{234}Th samples. After background count, filters were combusted in the Costech 4010 elemental combustion analyzer in the Scripps Institution of Oceanography (SIO) Analytical Laboratory. Prior to combustion, filters from the P0810 cruise were acidified to remove inorganic carbon. Filters from the P0704 cruise were not acidified, though comparisons of total and organic carbon flux collected in sediment traps on this cruise suggested that inorganic carbon flux was low (data not shown).

Sediment trap deployment and analyses

VERTEX-style drifting sediment traps (Knauer et al. 1979) were deployed on the drifter at the beginning and recovered at the end of each experimental cycle. Trap arrays consisted of 4 to 12 particle interceptor traps (PIT) with an inner diameter of 70 mm and aspect (height:diameter) ratio of 8:1. To create a semi-stable boundary layer immediately above the trap and minimize resuspension during recovery, each PIT had a baffle on top consisting of 14 smaller tubes with 8:1 aspect ratio. The baffle tubes were tapered at the top to ensure that all particles falling within the inner diameter of the PIT descended into the trap. On P0704, 8 PITs were deployed at a depth of 100 m during each cycle. On P0810, 8 to 12 PITs were deployed at 100 m, and 4 to 8 PITs were deployed near the base of the euphotic zone (50 or 60 m, except on Cycle 2, when the euphotic zone was close to 100 m).

Before deployment, each PIT was filled with a 2.2 l slurry composed of 0.1 µm filtered seawater with an additional 50 g l^{-1} NaCl to create a density interface within the tube that prevented mixing with *in situ* water. The traps were fixed with a final concentration of 4% formaldehyde before deployment to minimize decomposition as well as consumption by mesozoo-

plankton grazers (Knauer et al. 1984). Upon recovery, the depth of the salinity interface was determined, and the overlying water was gently removed with a peristaltic pump until only 5 cm of water remained above the interface. The water was then mixed to disrupt large clumps and screened through a 300 µm Nitex filter. Swimmers were removed from the filters under a dissecting scope. The remaining >300 µm non-swimmer particles were then combined with the total <300 µm sample. Samples were then split with a Folsom splitter, and subsamples were taken for C, N, C:^{234}Th, pigment analyses, and microscopy. Typically, subsamples of ¼ of the PIT tube contents were filtered through pre-combusted GF/F filters for organic carbon and nitrogen analyses. Filters were acidified prior to combustion in a Costech 4010 elemental combustion analyzer in the SIO Analytical Facility. Entire tubes were typically filtered through QMA filters for C:^{234}Th analyses as described above. Triplicate subsamples (typically 50 ml) were filtered, extracted in 90% acetone and analyzed for chlorophyll *a* (chl *a*) and phaeopigment concentrations using acidification with HCl and a Turner Designs Model 10 fluorometer (Strickland & Parsons 1972). Samples for microscopic analysis were stored in dark bottles and analyzed on land as described below.

Microscopic enumeration of sediment trap fecal pellets

On land, sediment trap samples were gently filtered through a 60 µm filter, then rinsed onto a gridded petri dish. These samples were analyzed under a Zeiss Discovery V12 dissecting microscope at 25× magnification (Wilson et al. 2008). Recognizable fecal pellets were separated from other sediment trap material and photographed under both bright- and dark-field illumination. Images were analyzed using ImagePro ver 6.0 (Media Cybernetics), with the bright-field images used to draw outlines around the fecal pellets. Dark-field images were used to determine color of the fecal pellets. Fecal pellets were manually classified into 6 different shape categories (ovoid, cylindrical, spherical, tabular, amorphous, and ellipsoid) with appropriate length and width relationships used to convert linear measurements into fecal pellet volumes. For tabular fecal pellets, we assumed that depth was equal to one half of width. Fecal pellets from several of the samples were sorted into broad classes (small, cylindrical, and tabular) and imaged for length and width measurements prior to combustion in a Costech 4010 elemental combustion analyzer to determine carbon:volume relationships. These resulted in mean carbon:volume conversion factors of 0.125 mg C mm^{-3} for ovoid, spherical and ellipsoid pellets, 0.055 mg C mm^{-3} for cylindrical and amorphous pellets, and 0.029 mg C mm^{-3} for tabular pellets. Fecal pellets (particularly tabular and cylindrical pellets) were often found broken, likely due to sample processing. When fragments were clearly recognizable, we counted these fragments as individual pellets. While this inflates the total number of pellets enumerated, it gives a good estimate of the total fecal pellet mass within the sample.

Mesozooplankton community enumeration

MOCNESS samples were analyzed to determine the concentrations and biomasses of broad taxa common in the CCE region (copepods, appendicularians, chaetognaths, salps and doliolids, eggs, euphausiids, nauplii, ostracods, polychaetes, pteropods, siphonophores, and others). Mesozooplankton were divided by size with a 1 mm filter, and each size-fraction was subsampled with a Folsom splitter until a reasonable amount of material (typically 100 to 1000 organisms) remained. An additional >5 mm fraction was analyzed to assess more accurately the larger animals in nighttime tows. Subsamples were analyzed using

Table 1. Mesozooplankton length:carbon relationships. For 'Others' we used an equation for hyperiid amphipods, which were the dominant contributor to this category

Taxa	Relationship: C(µg) = fn of length (µm) or volume (µm^3)	Source
Appendicularians	$0.49 \times (38.8 \times [l/1000]^{2.574})^{1.12}$	Lavaniegos & Ohman (2007)
Chaetognaths	$0.221 \times (l/1000)^{2.580}$	Gorsky et al. (2010)
Copepods	$0.461 \times (l/1000)^{3.094}$	Gorsky et al. (2010)
Doliolids	$0.51 \times (l/1000)^{2.28}$	Lavaniegos & Ohman (2007)
Eggs	$1.4 \times 10^{-7} \times$ Volume	Kiorboe & Sabatini (1995)
Euphausiids	$19.032 \times (l/1000)^{1.484}$	Gorsky et al. (2010)
Nauplii	$0.1489 \times (l/1000)^{2.588}$	Mauchline (1998)
Ostracods	$0.398 \times 17.072 \times (l/1000)^{2.545}$	Lavaniegos & Ohman (2007)
Polychaetes	$7.5 \times (l/1000)^{1.3848}$	Lavaniegos & Ohman (2007)
Pteropods	$0.221 \times 2.6 \times (l/1000)^{2.659}$	Lavaniegos & Ohman (2007)
Siphonophores	$20.47 \times (l/1000)^{0.834}$	Lavaniegos & Ohman (2007)
Others	$365 \times 10^{(-2.314 + 2.957 \times \log[l/1000])}$	Lavaniegos & Ohman (2007)

ZooScan hardware with ZooProcess and Plankton Identifier software (Gorsky et al. 2010). Following automated classification of organisms, all taxonomic identifications were manually checked and corrected, if necessary. Length (maximum feret diameter) and area measurements of each organism were used to estimate carbon weight using the relationships in Table 1.

Calculation of active carbon transport

Following ZooScan classification, the active transport of carbon by mesozooplankton that feed in the surface at night and respire at depth during the day was calculated for the dominant DVM taxa in the CCE region (copepods, euphausiids, chaetognaths, and others—noted to be primarily hyperiid amphipods). Since specific respiration is size-dependent, each taxon was binned into 11 size classes. The day-night biomass difference (integrated to 100 m depth) for each size class was then determined from paired MOCNESS tows (1 or 2 pairs of tows per cycle). Specific respiration rates for each size and taxonomic class were computed from the equation:

$$\text{Respiration } (\mu\text{l O}_2 \text{ ind.}^{-1} \text{ h}^{-1}) = e^{a_0 + a_1 \ln(CW) + a_2 T} \quad (1)$$

where CW is the carbon weight (mg C) and T is the average temperature (°C) from 100 to 450 m depth. The constants a_0, a_1 and a_2 were assumed to be 0.124, 0.780, and 0.073, respectively, for copepods (Ikeda et al. 2001) and 0.524, 0.835, and 0.061, respectively, for other metazooplankton (Ikeda 1985). This respiration rate is likely the organisms' standard metabolism, and hence may be an underestimate of their actual *in situ* metabolism. However, they were unlikely to be feeding at depth, and we believe their standard metabolism to be representative. We assumed that organisms respired at depth for 12 h per day. While we allowed individual size-classes to undergo both normal and reverse DVM, we assumed that bulk taxa (e.g. copepods and euphausiids) were not undergoing reverse DVM and hence set a minimum active transport rate of 0 for each taxa. The active transport of N was similarly calculated, using size-specific rates of ammonia excretion:

$$\text{Excretion } (\mu\text{g N ind.}^{-1} \text{ h}^{-1}) = e^{a_0 + a_1 \ln(CW) + a_2 T} \quad (2)$$

where CW and T are again carbon weight and average temperature and a_0, a_1, and a_2 are −2.769, 0.711, and 0.071, respectively, for copepods (Ikeda et al. 2001) and −2.176, 0.829, and 0.0648, respectively, for other metazooplankton (Ikeda 1985).

Since the dominant euphausiid species in our MOCNESS samples (*Euphausia pacifica, Nematoscelis difficilis*, and *Euphausia gibboides*) are known to be both strong vertical migrators and visual net-avoiders (Brinton 1967), we calculated an adjusted euphausiid active transport rate by assuming that daytime vertically-integrated euphausiid biomass (0 to 450 m) should be equal to night time biomass and that net avoidance was constant with depth. When daytime tows were deficient in integrated euphausiid biomass relative to paired nighttime tows, we scaled the daytime profile proportionally at all depths so that the integrated biomasses were equal and recalculated respiration at depth. This adjusted active transport rate may be an underestimate, as it does not take into account euphausiids that migrate deeper than 450 m; thus, the true transport rate may lie somewhere between the raw and adjusted rates.

Mesozooplankton gut pigment analyses

Daily rates of mesozooplankton community grazing on phytoplankton were determined from midday and midnight bongo tow samples. The samples were anesthetized with soda water and size-fractionated into size classes of 0.2–0.5, 0.5–1, 1–2, 2–5 and >5 mm. Each size-fraction was divided using a Folsom splitter, with 3/8 frozen in liquid nitrogen for gut fluorescence analyses. Subsamples of each size class were inspected under a dissecting microscope to remove phytoplankton and detritus, then sonicated in 90% acetone, centrifuged and read for chl *a* and phaeopigment concentrations using acidification on a Turner Designs Model 10 fluorometer.

As recommended by Conover et al. (1986), phaeopigment estimates were not multiplied by 1.51 (the chl *a*:phaeopigment ratio). Pigment degradation to non-fluorescent products was further assumed (following Durbin & Campbell 2007) to be included in determination of gut clearance rates. These clearance rates were estimated using the temperature dependent function K (min^{-1}) = 0.0124 $e^{0.0765T\ (°C)}$ of Dam & Peterson (1988), using mean temperature in the depth range of highest chlorophyll where zooplankton were expected to congregate and feed. To determine daily community ingestion rates, the sum of chl *a* and phaeopigments for all size-classes was averaged between day-night paired tows and multiplied by the gut pigment turnover rate to determine daily community ingestion rates. Gut pigment samples were not available for Cycles 5 and 6 of the P0810 cruise.

Statistical analysis

Throughout the manuscript, measurements are reported and plotted as mean ± standard deviation (SD), unless otherwise stated. When testing correlations between rate and standing stock measurements that both contain measurement error, we use the model II regression technique — geometric mean regression (Ricker 1973). To test the statistical significance of relationships between variables we use the non-parametric test — Spearman's rank correlation.

RESULTS

Cruise conditions

Nine quasi-Lagrangian drifter experiments (cycles) were conducted as part of this study (3 during spring upwelling conditions in April 2007, and 6 during late summer/fall conditions in October 2008; Fig. 1). The spring cruise (P0704) included 2 inshore cycles (Cycles 1 and 3) near the Point Conception upwelling source with significant surface nitrate concentrations (~5 and 7 µmol l^{-1}, for Cycles 1 and 3, respectively) and surface chlorophyll concentrations (>1 µg l^{-1}). Both of these cycles featured a large and active mesozooplankton community that impacted phytoplankton with high grazing rates (37.3 ± 14.0 and 7.7 ± 5.4 mg chl *a* m^{-2} d^{-1}, respectively) and drove an overall decrease in euphotic zone chlorophyll over the course of the 4 d experimental period (Landry et al. 2009). Cycle 2 took place in an offshore anticyclonic eddy with a low concentration of surface nitrate (<0.1 µM) and chlorophyll (~0.2 µg l^{-1}), a distinct deep chlorophyll maximum at ~70 m, and significantly lower mesozooplankton grazing (1.3 ± 0.5 mg chl *a* m^{-2} d^{-1}).

While October is typically a relatively quiescent period in the CCE, strong northerly winds beginning on 2 October during our P0810 cruise mixed surface waters near Point Conception, stimulating phytoplankton growth during Cycles 3 to 6. Surface nitrate was relatively low throughout all cycles (~0.15 to 0.3 µM) except for Cycle 5 (~2 µM), which was near the productive side of an upwelling front (Landry et al. 2012). Cycles 2 and 6 (the unproductive side of the front) were representative of more oligotrophic conditions, with low surface chlorophyll (~0.2 µg l^{-1}) and distinct subsurface chlorophyll maxima. While Cycle 1 occurred prior to the 2 October wind event and had a surface chlorophyll concentration of ~0.5 µg l^{-1}, Cycles 3 to 5 showed increasing chlorophyll from north to south (~0.7, 1.0, and 1.4 µg l^{-1}, respectively) suggesting net community growth as waters were advected southward. While Cycles 1 to 3 (like the cycles from P0704) averaged 4 d in length, Cycles 4 to 6 were shorter experiments of 2 d duration.

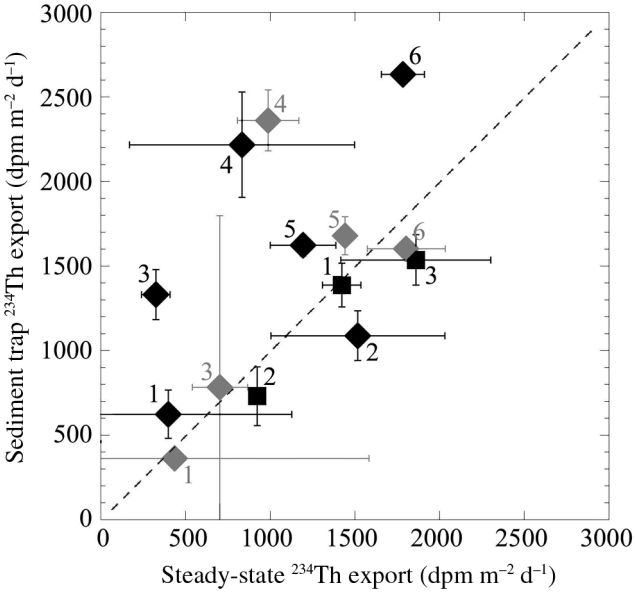

Fig. 2. Comparison of ^{234}Th export rates as estimated by ^{238}U-^{234}Th deficiency with a 1-dimensional steady-state equation that neglects upwelling (*x*-axis) and the amount of ^{234}Th collected in contemporaneous sediment traps (*y*-axis). Black symbols are at the 100 m depth horizon; gray are at the base of the euphotic zone (either 50 or 60 m). Squares are from cruise P0704; diamonds from P0810. Note good agreement is shown for all cycles except P0810-4, when strong northerly winds drove upwelling near Point Conception

Passive carbon export

We measured ^{234}Th activities on 2 to 3 casts per cycle. With the exception of one anomalous profile on P0810-1, vertical profiles consistently showed ^{234}Th deficiency at the surface and remineralization slightly below the base of the euphotic zone (Fig. 3). Repeated profiles showed no strong evidence of increasing deficiency over the 2 to 4 d experimental cycles. ^{234}Th export rates across the 100 m depth horizon (calculated using a simple 1-dimensional steady-state equation; Savoye et al. 2006) ranged from 325 to 1860 dpm m^2 d^{-1}, and were highest during the 2 nearshore cycles from P0704 and P0810-6, and lowest during P0810-1 and P0810-3. These steady-state ^{234}Th export rates closely matched ^{234}Th

fluxes determined from sediment traps placed at 100 m (and at the base of the euphotic zone on P0810), with the exception of Cycle P0810-4 (Fig. 2, Table 2). This latter cycle was started close to the Point Conception upwelling center shortly after a strong wind event moved through the region.

To convert ^{234}Th fluxes to carbon export, we measured the C:^{234}Th ratio on particles collected using 2 different methods: sediment traps and *in situ* pumps deployed at the same depth horizon. While the 2 collection methods determined the same broad patterns in the C:^{234}Th ratio, including higher C:^{234}Th in surface waters, they disagreed in the magnitude of the ratio (Fig. 4, Table 2). For most cycles, the *in situ* pump underestimated the C:^{234}Th ratio relative to the sediment trap, often by a factor of almost 2. In the

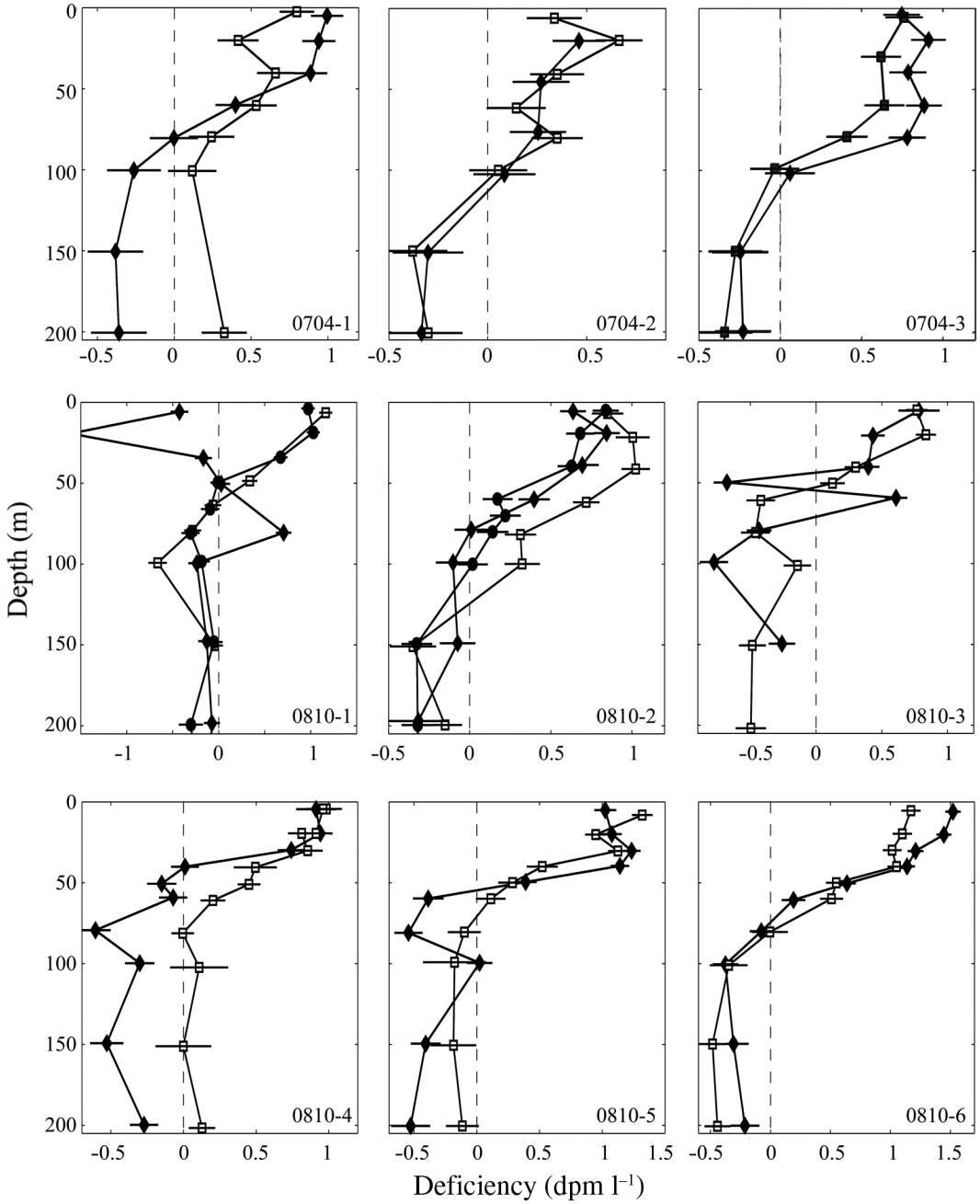

Fig. 3. ^{234}Th deficiency depth profiles, showing the deficiency of ^{234}Th relative to ^{238}U for our 9 experimental cycles (3 during cruise CCE-P0704 and 6 during cruise CCE-P0810). Error bars are propagation of measurement uncertainty. Diamonds, squares, and circles are replicate casts during a cycle (typically at beginning and end of cycle)

absence of an *a priori* reason to trust one method over the other, we used the average C:^{234}Th ratio determined by the 2 methods to compute steady-state estimates of passive carbon export (Table 3).

Table 2. Thorium measurements. Steady-state ^{234}Th export is calculated assuming a 1-dimensional steady-state model without vertical upwelling or diffusion. Sediment trap ^{234}Th export was the passive flux collected in VERTEX-style drifting particle interceptor traps (PIT), while sediment trap C:Th ratio was the C:^{234}Th ratio of these particles. *In situ* pump C:Th ratio was the C:^{234}Th ratio of size-fractionated particles collected by a McLane pump. Means ± standard deviations of replicate measurements are reported

	Depth (m)	Steady-state ^{234}Th export (dpm m^{-2} d^{-1})	Sediment trap ^{234}Th export (dpm m^{-2} d^{-1})	Sediment trap C:Th ratio (mg C dpm^{-1})	*In situ* pump C:Th ratio (mg C dpm^{-1})
0704-1	100	1423 ± 113	1388 ± 130	0.066 ± 0.005	0.042 ± 0.004
0704-2	100	922 ± 50	731 ± 174	0.043 ± 0.010	0.026 ± 0.002
0704-3	100	1860 ± 442	1537 ± 149	0.087 ± 0.014	0.044 ± 0.012
0810-1	100	398 ± 728	624 ± 142	0.129 ± 0.021	0.033 ± 0.012
	50	437 ± 1146	363 ± 35	0.247 ± 0.035	0.095 ± 0.073
0810-2	100	1518 ± 514	1088 ± 147	0.039 ± 0.002	0.027 ± 0.015
0810-3	100	325 ± 84	1331 ± 148	0.050 ± 0.002	0.062 ± 0.065
	60	703 ± 164	783 ± 1014	0.067 ± 0.013	0.038
0810-4	100	834 ± 665	2218 ± 311	0.063 ± 0.011	0.048
	50	989 ± 182	2362 ± 180	0.094 ± 0.008	0.066 ± 0.017
0810-5	100	1194 ± 194	1622 ± 62	0.061 ± 0.008	0.029
	60	1442 ± 51	1679 ± 112	0.103 ± 0.013	0.054 ± 0.010
0810-6	100	1784 ± 128	2634 ± 13	0.036 ± 0.004	0.024 ± 0.001
	60	1803 ± 231	1603 ± 33	0.065 ± 0.020	0.079

For the 9 experimental cycles, steady-state carbon export averaged 54 mg C m^{-2} d^{-1} (range 18 to 121) at the 100 m depth horizon (Table 3). On the P0704 cruise onshore cycles had export rates of 77 ± 11 and 121 ± 45 mg C m^{-2} d^{-1} (P0704-1 and P0704-3), while the offshore cycle had substantially lower export of 32 ± 10 mg C m^{-2} d^{-1}. On P0810, export was much less variable (mean across cycles of 42 ± 14) and showed no distinct trends with distance from shore. A comparison of Th-derived export at the 100 m depth horizon to export at the base of the euphotic zone (50 to 60 m) showed substantial remineralization, with an average of 52 ± 7% of carbon remineralized between the euphotic zone and 100 m depth. Our paired sediment traps, by comparison, showed only 21 ± 17% of carbon was remineralized in this depth horizon. Regardless, remineralization was substantial, hence the calculated carbon export for the P0704 cruise (when we only measured export at 100 m) should be considered lower bounds for carbon flux across the base of the euphotic zone.

Table 3. Sediment trap (ST) flux measurements. The first flux column is organic carbon (Corg) export computed from ^{234}Th:^{238}U deficiency multiplied by the mean of the 2 C:^{234}Th ratios of particles collected by *in situ* pumps and sediment traps. Last column is percentage of recognizable fecal pellet carbon in sediment traps. All other columns are mass fluxes determined by sediment trap (mean ± standard error, where shown). Chl: chlorophyll; phaeo: phaeopigment. Sample sizes ranged from 3 to 5 for most rates, except for thorium deficiency (2 profiles per cycle) and fecal pellet mass measurements (2 subsamples sorted per sediment trap). GeoMean is the geometric mean of values at the base of the euphotic zone (includes 100 m values from cycles when we only deployed traps at one depth) or at 100 m. –: no data collected

Cycle	Depth (m)	^{234}Th Corg (mg C m^{-2} d^{-1})	ST Corg (mg C m^{-2} d^{-1})	ST N (mg N m^{-2} d^{-1})	Chl (µg m^{-2} d^{-1})	Phaeo (µg m^{-2} d^{-1})	Fecal pellet mass flux (mg C m^{-2} d^{-1})	(% ST C flux)
P0704-1	100	77 ± 11	144 ± 12.7	22.2 ± 4	443 ± 245	3501 ± 816	135.2	93.9
P0704-2	100	32 ± 10	32 ± 6.3	7.6 ± 1.6	19 ± 2	146 ± 48	3.6	11.3
P0704-3	100	121 ± 45	170 ± 40.8	30.0 ± 8.6	407 ± 153	3449 ± 701	53.6	31.5
P0810-1	100	32 ± 60	74 ± 10.6	9.0 ± 0.8	47 ± 19	529 ± 133	4.4	5.9
P0810-1	50	75 ± 199	112 ± 34.4	13.8 ± 5.7	17 ± 7	337 ± 128	6.7	6
P0810-2	100	51 ± 29	69 ± 12.8	7.7 ± 1.3	–	–	7.6	11
P0810-3	100	18 ± 22	78 ± 6.6	10.2 ± 0.9	12	217	5	6.4
P0810-3	60	37 ± 13	120 ± 12.5	15.3 ± 2.8	31 ± 20	331 ± 235	22.6	18.8
P0810-4	100	46 ± 38	149 ± 36.3	14.4 ± 3.9	266 ± 97	2723 ± 232	35.4	23.8
P0810-4	50	79 ± 24	216 ± 4.4	25.7 ± 0.7	426 ± 116	4214 ± 597	80.4	37.2
P0810-5	100	53 ± 13	127 ± 21.7	12.4 ± 1.7	123 ± 43	1141 ± 76	14.1	11.1
P0810-5	60	113 ± 24	128 ± 27.3	13.9 ± 3.8	251 ± 43	1575 ± 145	25.9	20.2
P0810-6	100	54 ± 8	107 ± 5	8.9 ± 1	34 ± 9	211 ± 52	3.5	3.3
P0810-6	60	130 ± 40	112 ± 12.3	10.8 ± 1.7	66 ± 7	438 ± 175	5.1	4.6
GeoMean	Euph	71.5	109.4	14.7	103.1	932.5	19	17.3
GeoMean	100	47.1	95.0	12.1	82.5	776.9	12.5	13.2

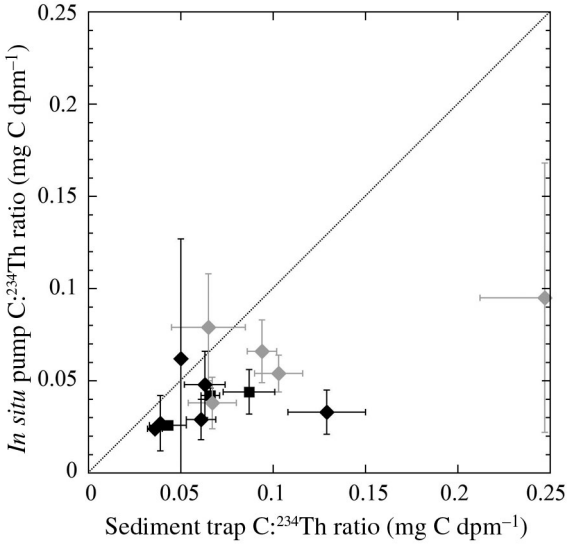

Fig. 4. C:^{234}Th ratios. *X*-axis is the C:^{234}Th ratio measured on particles caught in sediment traps; *y*-axis is the same ratio measured using *in situ* pumps and size-fractionated particles >20 µm (cruise P0704) or >50 µm (P0810). Black symbols are traps at 100 m depth; gray are base of the euphotic zone (50 or 60 m). Squares are P0704; diamonds P0810. Dotted line is the 1:1 line

Sediment trap contents

Trap carbon and nitrogen samples (Table 3) showed that the molar C:N ratios on sinking material averaged 6.4 during the spring cruise, similar to the C:N ratio of particulate organic matter (POM) in the euphotic zone (6.1). While the C:N ratio of POM in surface water in the fall was not significantly different, the sinking material was depleted in nitrogen, with average C:N ratios of 10.2 at the base of the euphotic zone and 11.1 at 100 m, suggesting substantial reworking of sinking POM. The magnitude of total pigment flux was highly variable, but phaeopigment flux was consistently an order of magnitude higher than chl *a* flux (Fig. 5). Pigment fluxes indicate that bulk phytoplankton sinking rates never exceeded 0.66 m d^{-1} (with an average across all cycles of 0.23 m d^{-1}). This is likely an overestimate as the low chl:Phaeo ratios suggest that a substantial portion of the sediment trap chlorophyll sank undegraded in fecal pellets. Bulk phaeopigment sinking rates ranged from 0.71 to 18.6 m d^{-1} (with an average of 5.0 m d^{-1}). Phaeopigment flux into sediment traps was strongly correlated with flux of recognizable fecal pellets (Fig. 6), the presumptive source of the digestion-degraded chlorophyll. Pigment fluxes were highest during Cycles P0704-1 and P0704-3 when large herbivorous mesozooplankton were abundant.

Two sediment trap samples from each trap deployment and depth were microscopically sorted at 25× magnification to characterize the >60 µm particle

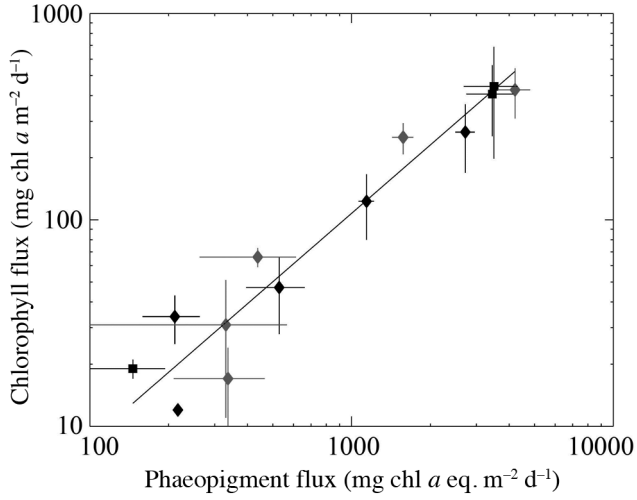

Fig. 5. Chlorophyll *a* flux (mg chl *a* m^{-2} d^{-1}) and phaeopigment flux (Ph) collected in sediment traps (mg chl *a* equivalent m^{-2} d^{-1}). Black symbols are traps at 100 m depth; gray are base of the euphotic zone (50 or 60 m). Squares are cruise P0704; diamonds P0810. Black line is the model II regression: log(chl) = −2.9 + 1.1 × log(Ph). Spearman's rank correlation shows the correlation between chl and Ph to be significant ($p = 9.9 \times 10^{-6}$)

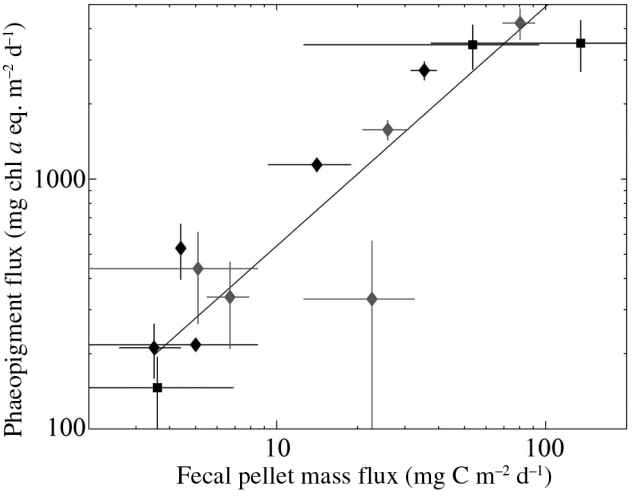

Fig. 6. Phaeopigment flux (Ph, mg chl *a* eq. m^{-2} d^{-1}) and mass flux of recognizable fecal pellets (FP, mg C m^{-2} d^{-1}). Black symbols are traps at 100 m depth; gray are base of the euphotic zone (50 or 60 m). Squares are cruise P0704; diamonds are P0810. Black line shows a model II regression: log(Ph) = 4.1 + 0.96 × log(FP). Spearman's rank correlation shows the correlation between Ph and FP to be significant ($p = 4.6 \times 10^{-5}$)

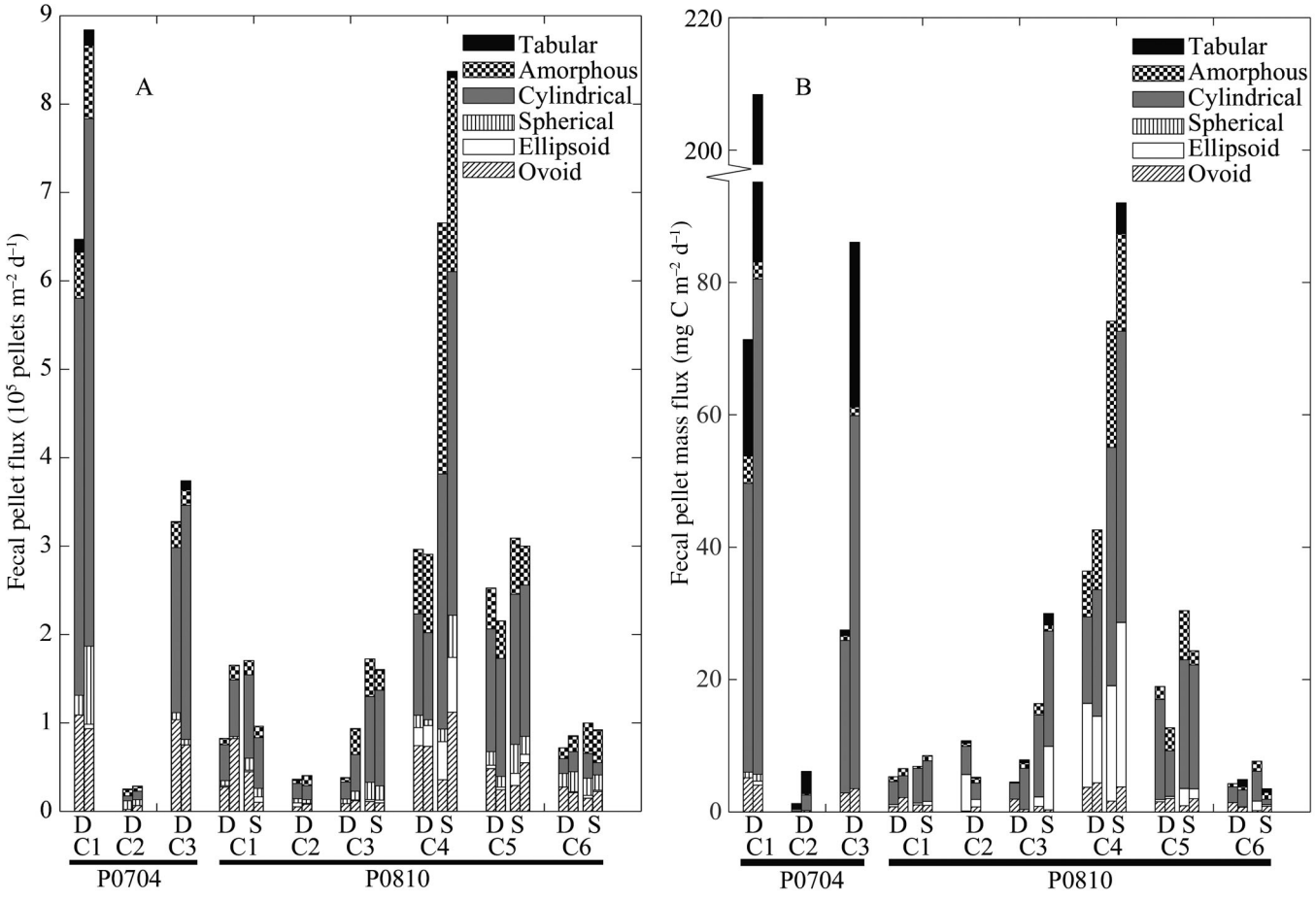

Fig. 7. Fecal pellet flux. (A) Flux of recognizable fecal pellets into sediment traps (10^5 pellets m^{-2} d^{-1}). (B) Carbon flux of recognizable fecal pellets (mg C m^{-2} d^{-1}). Samples are grouped by cruise, cycle and depth ('D' denotes deep samples from 100 m; 'S' denotes shallow samples from base of euphotic zone; 50 or 60 m). Paired samples from each cycle and depth are shown adjacent to each other. Shading indicates shape of fecal pellets

size-fraction. In addition to quantitative analysis of fecal pellet flux, we qualitatively assessed the relative contributions of visible material (marine snow, fecal pellets, and smaller unidentifiable particles) to sample biovolume. Fecal pellets were the visibly dominant component in sediment trap samples from P0704-1. For P0704-2, numerous small zooplankton made it through the 303 µm mesh screen; thus, we believe that organic carbon flux was overestimated on that cycle. For the 2 samples from P0704-3, a significant portion of one was comprised of marine snow containing fragments of degraded fecal pellets, and the other sample was primarily fecal pellets. Recognizable fecal pellets were not common in any of the samples from P0810-1, with the surface samples dominated by marine snow aggregates and the deeper samples comprised mainly of small unidentifiable particles. For P0810-2, one sample was pellet dominated while the other contained mostly large fluffy white aggregates of marine snow. The P0810-3 surface samples contained primarily marine snow while the deep samples contained little material. Overall, fecal pellets dominated the flux of particulate material during cycles in productive water, while the proportion of recognizable material was lower for cycles in the more oligotrophic regions.

Enumeration of recognizable fecal pellets uncovered several distinct patterns. Although recognizable fecal pellets were a small proportion of the passive flux in most cycles (median = 11%), they contributed 25% of measured passive flux due to their dominance during productive periods. Across all cycles, cylindrical fecal pellets—presumably egested by euphausiids or large copepods—were the most

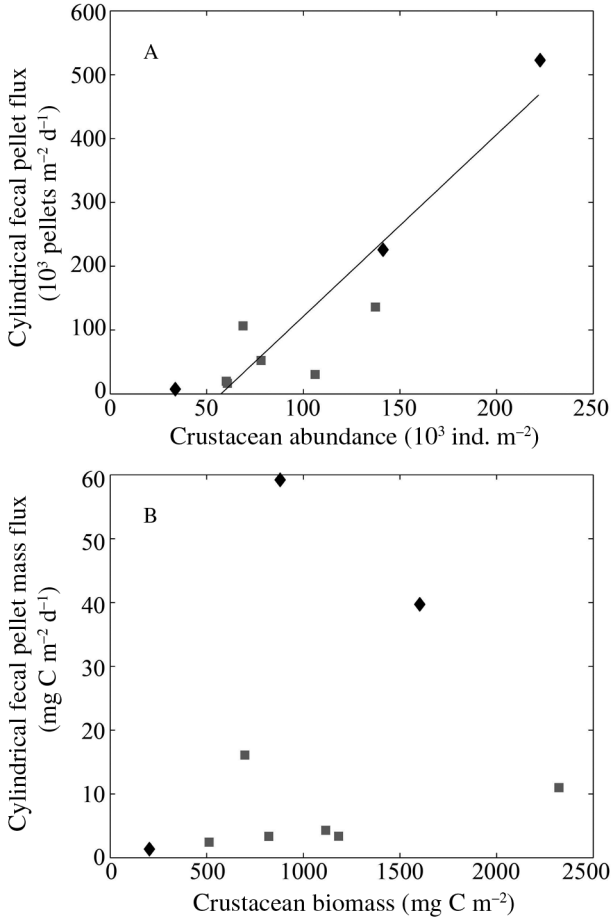

Fig. 8. Relationship between cylindrical fecal pellets and total crustacean abundance. (A) Crustacean abundance (CA) (day-night average from MOCNESS tows integrated to 100 m) and cylindrical fecal pellet flux (FP, at 100 m). (B) Crustacean biomass and fecal pellet mass flux. Gray squares are cruise P0704; black diamonds are P0810. Model II regression line in panel (A) is: $FP = -1.6 \times 10^5 + 2.8 \times 10^3 \times CA$. Spearman's rank correlation shows the correlation between FP and CA to be significant ($p = 5.1 \times 10^{-4}$)

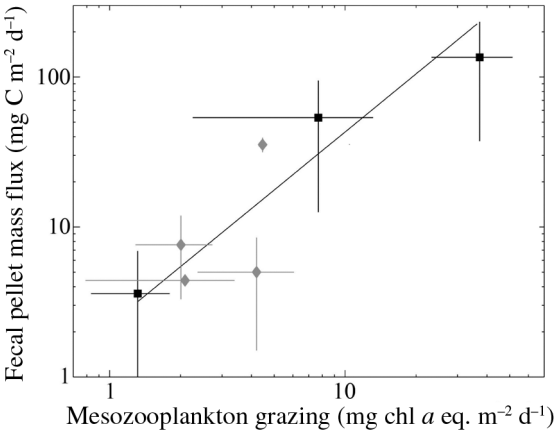

Fig. 9. Relationship between fecal pellet mass flux (FP, mg C m^{-2} d^{-1}), at 100 m depth, and mesozooplankton grazing rates (mg chl *a* eq. m^{-2} d^{-1}) as determined from gut pigment analyses of day-night paired bongo tows. Error bars show the range of paired measurements. Black squares are cruise P0704; gray diamonds are P0810. Line is model II regression: log(FP) = 0.8 + 1.3 × log(grazing). Spearman's rank correlation shows the correlation between fecal pellet mass flux and grazing to be significant (p = 0.0068)

abundant pellet type (Fig. 7a) and also typically the dominant source of recognizable fecal pellet carbon (Fig. 7b). However, tabular (salp) fecal pellets, while never abundant, were a significant source of particulate organic carbon (POC) when present. In particular, 1 of the 2 samples from P0704-1 contained enough tabular fecal pellet carbon (125 mg C m^{-2} d^{-1}) to exceed the total flux of carbon measured in most of the trap deployments. The important, but variable, nature of their contribution to total flux highlights the difficulties in assessing complete budgets of sinking material. Small ovoid fecal pellets (believed to be appendicularian egesta) contributed a consistently small portion of fecal pellet abundance (20% on average) and mass (12%). A strong correlation was found between crustacean abundance and their cylindrical fecal pellets (Fig. 8, $p = 5.1 \times 10^{-4}$). In contrast, no statistically significant correlation was found between crustacean biomass and fecal pellet biomass ($p > 0.05$), likely because biomass variability was driven by larger organisms and larger pellets that were sampled less accurately. We found no correlations between salps and appendicularians and their respective fecal pellets, likely because neither taxon was abundant in the MOCNESS samples. However, mesozooplankton grazing rates measured by the gut fluorescence technique were strongly correlated with fecal pellet mass flux (Fig. 9, p = 0.0068).

Active transport by DVM mesozooplankton

While sediment traps and ^{234}Th disequilibrium measurements only account for the flux of organic carbon on passively sinking particles, vertically migrating mesozooplankton also actively transport carbon to depth by feeding in the euphotic zone at night and respiring at depth during the day. We assessed day-night vertical distributions of common mesozooplankton taxa from the collections of paired day-night MOCNESS tows to 450 m (with typical 50 m vertical resolution) combined with ZooScan

Table 4. Active transport by diel vertically migrating mesozooplankton

	Copepods	Euphausiids	Euphausiids[a]	Chaetognaths	Others (Hyperiids)	Total	Total[a]
Carbon transport by respiration (mg C m^{-2} d^{-1})							
0704-1	10.0	10.4	5.4	0	0.3	20.6	15.6
0704-2	1.9	1.4	0.6	0.5	0	3.8	3.0
0704-3	1.8	47.5	40.6	0.3	0.1	49.8	42.8
0810-1	16.3	8.0	4.9	0	2.5	26.8	23.7
0810-2	3.4	5.2	4.3	0.8	5.3	14.7	13.8
0810-3	9.0	4.7	3.5	0	4.5	18.2	17.0
0810-4	3.7	0	0	2.6	0	6.3	6.3
0810-5	9.7	55.5	35.7	0.2	1.5	66.9	47.1
0810-6	0	2.4	2.4	0	0	2.4	2.4
Nitrogen transport by excretion (mg N m^{-2} d^{-1})							
0704-1	1.45	1.35	0.70	0	0.04	2.83	2.18
0704-2	0.25	0.18	0.08	0.06	0	0.49	0.39
0704-3	0.29	6.27	5.35	0.05	0.02	6.62	5.70
0810-1	2.18	1.04	0.65	0	0.32	3.55	3.15
0810-2	0.47	0.68	0.57	0.11	0.68	1.94	1.82
0810-3	1.34	0.61	0.45	0	0.58	2.53	2.37
0810-4	0.43	0	0	0.34	0	0.76	0.76
0810-5	1.44	7.18	4.62	0.03	0.20	8.85	6.29
0810-6	0	0.31	0.31	0	0	0.31	0.31

[a]Adjusted euphausiid active transport value, which takes into account possible daytime net avoidance behavior

analysis of the mesozooplankton assemblage in each net. We focused on 4 broad taxonomic groups that had both high abundances and strong DVM behaviors: copepods (Fig. S1 in the Supplement at www.int-res.com/articles/suppl/m491p047_supp.pdf), euphausiids (Fig. S2 in the Supplement), chaetognaths (Fig. S3 in the Supplement), and our 'other' category (Fig. S4 in the Supplement), which was comprised primarily of hyperiid amphipods.

A comparison of the day-night differences in abundance showed consistent deficiency of surface daytime populations relative to nighttime populations, particularly for copepods and euphausiids (Figs. S1 & S2 in the Supplement). For most populations, a euphotic zone deficiency in daytime biomass was matched by a subsurface increase, providing confidence that organisms were actually migrating to depth and that our results were not due to either sampling biases or random variations in patchy populations. However, we noticed that vertically integrated (0 to 450 m) estimates of euphausiid biomass were often substantially higher at night than during the day (geometric mean of night/day biomass = 2.1), suggesting that these visually acute animals were actively avoiding the MOCNESS net during the day. We corrected for this overestimate of euphausiid DVM by scaling up the daytime profile by a constant fraction so that daytime and nighttime biomasses were equal. We

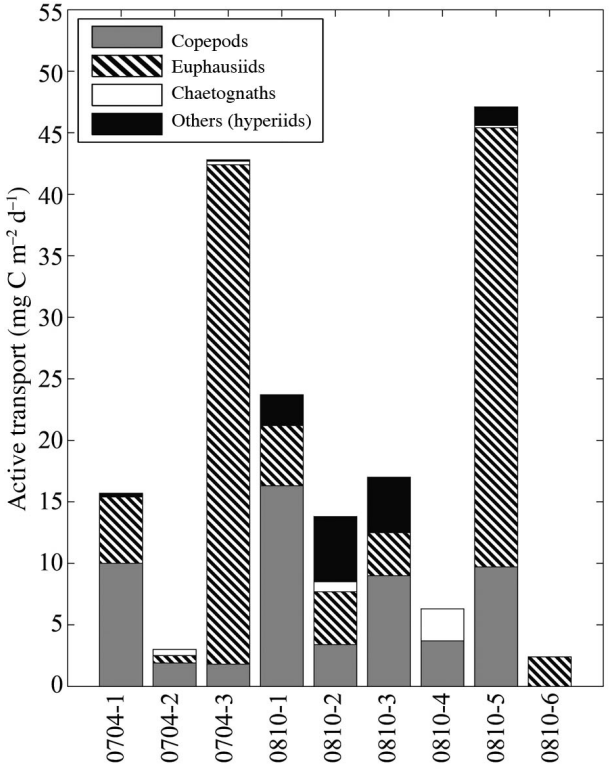

Fig. 10. Active transport of carbon (mg C m^{-2} d^{-1}) by vertically migrating mesozooplankton across 100 m depth: copepods, euphausiids, chaetognaths and 'others' (primarily hyperiid amphipods) are represented. Euphausiids are corrected for net avoidance (see 'Materials and methods')

found no evidence for migratory behaviors for siphonophores and for combined salps and doliolids, largely because these groups were seldom found in the MOCNESS samples.

Active transport by mesozooplankton varied from 2.4 to 47.1 mg C m^{-2} d^{-1} (mean across cycles of 19.1 ± 16.3) and was driven by the DVM of copepods and euphausiids (Table 4, Fig. 10). Copepods typically accounted for half of active transport, but the euphausiid contribution was highly variable. Particularly high euphausiid active transport rates of 40.6 and 35.7 mg C m^{-2} d^{-1} (Cycles 0704-3 and 0810-5, respectively) were associated with high abundances of the largest size classes (>7 mm for 0704-3 and >10 mm for 0810-5), which were strong diel migrators whenever present. A positive correlation with surface chlorophyll was found ($p = 0.036$), though it described only 41% of the variability in active transport. Active carbon transport was a relatively constant fraction of surface nighttime biomass, averaging 9×10^{-6} mg C d^{-1} mg C^{-1} (varying from 4×10^{-6} to 1.5×10^{-5}). Active nitrogen transport followed a very similar pattern to carbon transport (Table 4), with an average C:N mass ratio of 7.6:1.

DISCUSSION

Passive export flux measurements

Methodological uncertainties with both sediment traps and ^{234}Th disequilibrium make POC fluxes difficult to constrain (Burd et al. 2010). Sediment trap inaccuracies can arise from hydrodynamic bias, swimmer contamination, and solubilization within the trap (Buesseler et al. 2007). Uncertainties in the radionuclide disequilibrium technique arise from the steady-state assumption, neglecting vertical and horizontal advective fluxes (Savoye et al. 2006) and variable C:radionuclide ratios of sinking particles (Buesseler et al. 2006).

Despite these difficulties, the 2 techniques yielded similar results in the present study, providing some measure of validation to the passive carbon export measurements. In particular, the measured flux of ^{234}Th into our drifting traps agreed well with the steady-state model of ^{234}Th export rates (Fig. 2, $r^2 = 0.52$ when P0810-4 is excluded). For the cycle when the 2 methods disagreed (P0810-4), we hypothesize that the discrepancy was likely due to a non-steady state wind-induced upwelling event near Point Conception. Assuming a modest upwelling term of 0.7 m d^{-1} (for comparison, Rykaczewski & Checkley 2008 computed upwelling rates in our region ranging from –0.5 to 2.5), combined with the vertical gradient in ^{234}Th of 0.012 dpm l^{-1} m^{-1}, makes the steady-state disequilibrium calculations and sediment trap measurements of ^{234}Th flux at 100 m compatible for this cycle.

Unlike the similarity observed in ^{234}Th flux measurements, a distinct difference was found between the C:^{234}Th ratios determined by sediment traps and *in situ* pumps (Fig. 4), with sediment trap ratios averaging 1.6 times higher (geometric mean) than those ratios measured with the *in situ* pumps. This difference could be a simple consequence of the pumps oversampling slowly sinking particles. Such particles have more time to equilibrate with deeper water conditions where POC to total thorium ratios are substantially higher than at the surface, thus deflating their C:^{234}Th ratio relative to rapidly sinking particles. Furthermore, while *in situ* pump and sediment trap samples experienced similar decreases in C:^{234}Th with depth (geometric mean of the ratio of deep:shallow C:^{234}Th ratios was 0.61 for sediment traps and 0.58 for *in situ* pumps), the decrease with depth was far more variable for the pump samples (range of ratio of deep:shallow was 0.52 to 0.74 for sediment traps and 0.29 to 1.63 for pumps). This suggests that the sediment trap samples were more representative of the sinking particle flux, consistent with the hypothesis that pumps may oversample slowly sinking particles. Despite the attractiveness of this simple explanation, not all studies comparing sediment traps to pumps give the same result, likely due to differences in regional food web dynamics (e.g. Benitez-Nelson et al. 2001a).

While we cannot address hydrodynamic or solubilization biases of sediment traps with the present data, our microscopic sorting of fecal pellet contents allowed us to assess the impact of swimmer contamination. In general, screening with a 303 µm filter and microscopically sorting the larger size-fraction efficiently removed mesozooplankton from the samples. However, during microscopic analyses for fecal pellet enumeration, substantial (but unquantified) contamination by small swimmers was found in samples from oligotrophic cycle P0704-2 (also P0810-1, P0810-3 and P0810-6 to lesser extents). In P0704-2, swimmers likely comprised at least 50% of sample carbon, leading to an overestimate of carbon flux by a factor of 2 or more. Relative to the steady-state calculation, these particular sediment traps therefore actually underestimated ^{234}Th flux. However, since mesozooplankton swimmers were found

to have very high C:^{234}Th ratios (data not shown), they would not have contributed much thorium to the trap samples.

Contribution of fecal carbon to vertical flux

Previous studies have established that fecal pellet production is sufficient to drive passive vertical carbon export in the CCE (Landry et al. 1994, Stukel et al. 2011). For example, Stukel et al. (2011) showed with a simple trophic model based on measured rates of growth and grazing and assumed 30% egestion efficiency that mesozooplankton egestion could account for all of the variability in measured passive carbon export across a production gradient from coastal upwelling to offshore oligotrophic waters. Similarly, inverse ecosystem models indicate that combined zooplankton grazing processes can account for 65 to 95% of vertical flux (Stukel et al. 2012). In the present study, we used 2 different approaches to assess experimentally the contribution of fecal pellets to carbon export: microscopic enumeration of recognizable pellets and pigment analysis of trap samples.

If all ingested chlorophyll is converted to phaeopigments and none is lost to non-fluorescent particles, the carbon content of fecal pellets (FP) derived from recent herbivory (h) can be calculated as:

$$C_{\mathrm{FP,h}} = Ph \times C:chl \times \frac{(1-AE)}{CE} \quad (3)$$

where *Ph* is the phaeopigment concentration, *C:chl* is the carbon to chlorophyll ratio of mesozooplankton prey, *AE* is the assimilation efficiency of mesozooplankton, and *CE* is the conversion efficiency of chl *a* to phaeopigments. For *CE* = 1 (quantitative conversion of chl *a* to phaeopigments; Downs & Lorenzen 1985) and the assimilation efficiencies calculated by Stukel et al. (2012), the present trap results would indicate that mesozooplankton herbivory is responsible for 1.4 to 37% of vertical carbon flux, with a weighted average across all cycles of 12% (Table 5). This estimate is likely conservative, however, as mesozooplankton digestive degradation of pigments to non-fluorescent molecules is a well demonstrated process (Conover et al. 1986, Penry & Frost 1991, Goericke et al. 2000). Penry & Frost (1991) found that *CE* depends on food concentration, with low-food acclimated copepods converting significantly less chlorophyll to non-fluorescent molecules (8%) than high-food acclimated copepods (53%). Similarly, Goericke et al. (2000) found that CCE copepods and euphausiids converted ~55% of chl *a* to non-fluores-

Table 5. Contribution of phytoplankton and fecal pellets to vertical flux as assessed from pigment analyses. Vertically integrated (vert. int.) phytoplankton biomass was assessed using epifluorescence microscopy (Taylor et al. 2012). Phyto C flux is calculated as the product of chl flux and C:chl ratio. AE is the assimilation efficiency of the mesozooplankton (Stukel et al. 2012 for P0704 and Conover 1966 for P0810). Herbivorous (herb.) fecal flux is calculated either assuming no pigment degradation (lower) or assuming that 55% of the pigment is degraded (upper). Percent phyto is the percentage of phytoplankton in the prey of mesozooplankton (Stukel et al. 2012) and is used to calculate non-pigmented and hence total fecal flux for the 2007 cruise (the only cruise for which Stukel et al. 2012 provides percent phyto). ST: sediment trap

	Depth (m)	ST C export (mg C m^{-2} d^{-1})	Vert. int. phyto biomass (mg C m^{-2})	Vert. int. chl (mg chl m^{-2})	Phyto C flux (mg C m^{-2} d^{-1})	AE	Herb. fecal flux (lower) (mg C m^{-2} d^{-1})	Herb. fecal flux (upper) (mg C m^{-2} d^{-1})	% Phyto	Total fecal flux (lower) (mg C m^{-2} d^{-1})	Total fecal flux (upper) (mg C m^{-2} d^{-1})
P0704-1	100	144	2613	67	17.3	0.61	53.6	119.0	72	74.8	191.3
P0704-2	100	32	2079	31	1.3	0.66	3.3	7.2	22	14.9	44.3
P0704-3	100	170	2239	78	11.7	0.69	31.4	69.7	56	56.4	179.1
P0810-1	100	74	748	56	0.6	0.7	2.1	4.7			
P0810-1	50	112	748	56	0.2	0.7	1.3	3.0			
P0810-2	100	69	609	22							
P0810-3	100	78	644	39	0.2	0.7	1.1	2.4			
P0810-3	60	120	644	39	0.5	0.7	1.6	3.7			
P0810-4	100	149	2340	68	9.1	0.7	28.1	62.4			
P0810-4	50	216	2340	68	14.6	0.7	43.4	96.5			
P0810-5	100	127	961	65	1.8	0.7	5.0	11.2			
P0810-5	60	128	961	65	3.7	0.7	7.0	15.5			
P0810-6	100	107	396	19	0.7	0.7	1.3	2.9			
P0810-6	60	112	396	19	1.4	0.7	2.7	5.9			

cent molecules. Using this more liberal estimate of *CE* (0.45), 3 to 83% of passive carbon export is derived from recent mesozooplankton herbivory, with an average of 26% for all cycles. Since this only represents the fecal flux from herbivorous feeding, we can extrapolate to total flux of fecal carbon using the estimated ratio of phytoplankton to total mesozooplankton consumption calculated from inverse models for the P0704 cruise (Stukel et al. 2012). With this correction, fecal pellets contribute at least 52, 47 and 33% of vertical flux for P0704 Cycles 1, 2 and 3, respectively, using lower estimates from the Downs & Lorenzen (1985) equation (Table 5). If we assume, as above, that more than half of the ingested pigments are degraded to non-fluorescing material during digestion, fecal flux can easily account for all vertical carbon flux collected in 100 m traps during the spring cruise.

For comparison, we can calculate the proportion of flux derived from gravitational sinking of ungrazed phytoplankton by multiplying the C:chl *a* ratio by chl *a* flux into the sediment traps, although this is likely to be an overestimate as some ingested chlorophyll passes through mesozooplankton guts without conversion to phaeopigments (Downs & Lorenzen 1985). This calculation suggests that direct phytoplankton sinking contributes only 0.2% to 13% of vertical flux, with an average of 4% across all cycles. Considering that the chl *a* flux never exceeded 14% of total pigment flux, it is possible that pellets account for all of the measured chl *a* as well as phaeopigment flux.

Direct assessment of the contribution of fecal pellets to vertical flux is complicated by processes that mask the fecal origin of material in sediment traps (Turner 2002), including fragmentation of pellets both in the water column and during sample processing and not accounting for their contributions to marine snow aggregates. Additionally, small <60 µm pellets, produced by metazooplankton nauplii and microzooplankton (Gowing & Silver 1985), would not have been sampled by our methods, but are unlikely to sink rapidly or contribute significantly to total export. In our trap collections, carbon density (carbon:biovolume) was higher for smaller pellets, decreasing from 0.125 mg C mm^{-3} for small ovoids, spheres, and ellipsoids to 0.055 mg C mm^{-3} for cylindrical pellets and 0.029 mg C mm^{-3} for tabular pellets. Thus, the least visually conspicuous pellets in traps could be disproportionately high in carbon. Despite these conservative biases, recognizable fecal pellets are a significant source of carbon flux in the CCE region. Though they represented 50% of mass flux in only 2 of the trap samples, they accounted for ~25% of total flux across the 100 m depth horizon in the 9 experimental cycles due to their dominant role during higher export periods.

Role of mesozooplankton in vertical carbon flux

Mesozooplankton can mediate biogeochemical fluxes in both direct and indirect ways. Though highly variable (Small & Ellis 1992, Gowing et al. 2001, Wilson et al. 2008), their fecal pellets are often the dominant recognizable contents in sediment traps (Turner 2002). Their grazing impacts can regulate the total production of particles in the surface ocean, as observed in net negative rates of phytoplankton growth for nearshore Cycles 1 and 3 during P0704 (Landry et al. 2009). They transform sinking material by feeding on their own fecal pellets (Gowing & Wishner 1986) and marine snow aggregates (Wilson et al. 2010). In addition to their role in passive transport, active DVM behavior by mesozooplankton plays an important role in transporting carbon and nitrogen to depth, especially in oligotrophic regions (Longhurst et al. 1990, Steinberg et al. 2000, Al-Mutairi & Landry 2001).

By simultaneously assessing total particle flux by 2 methods (sediment traps and ^{234}Th), as well as the fluxes of recognizable fecal pellets, pigments, and DVM active transport, we were able to compare and constrain the contributions of mesozooplankton to total carbon export in the CCE during April 2007 and October 2008 (Fig. 11). Across all experimental cycles, the gravitational sinking of ungrazed phytoplankton was only a minor portion of total flux. During the spring cruise, fecal pellets likely comprised the majority of all sinking material. In the fall, however, identifiable pellets accounted for significantly less trap material while total export was not significantly different than in spring. In particular, marine snow dominated flux during Cycles 1 to 3. Decreased importance of recognizable fecal pellets and phaeopigments under less productive conditions may result from greater residence time of fecal material in the surface layer, allowing increased physical and biological disruption of pellets. Contrary to expectations (e.g. Takahashi et al. 2009), the ratio of active to passive carbon export did not vary inversely with productivity. Across all cycles, active transport averaged 19% (range 3 to 50%) of total carbon export across the 100 m depth horizon, stemming primarily from the DVM of copepods and euphausiids. Spatial variability in active transport was largely driven by

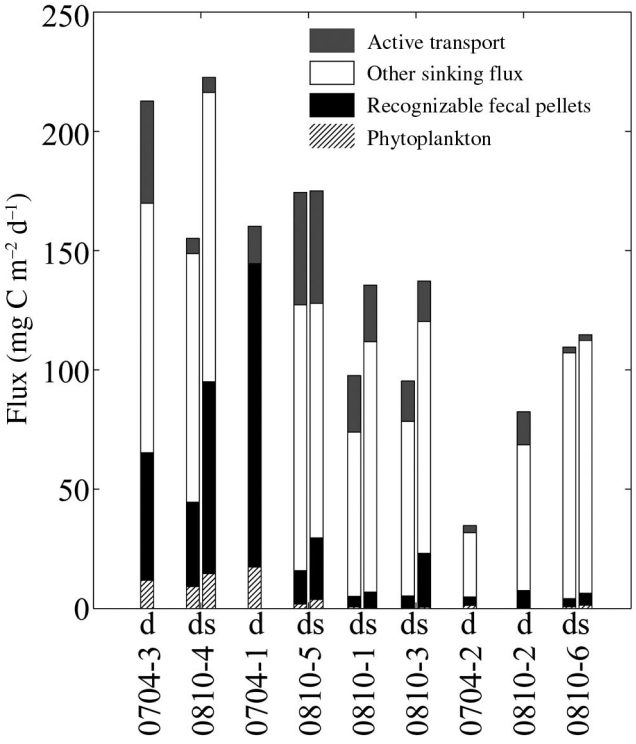

Fig. 11. Contribution of flux components to total carbon export. Recognizable fecal pellets are a lower limit for total fecal pellet flux. Phytoplankton flux is an overestimate because significant chlorophyll may have been transported in fecal pellets. Other sinking flux is portion of total trap flux not accounted for by recognizable fecal pellets and phytoplankton. When the sum of recognizable components exceeded total measured flux (0704-1), each component was scaled proportionally to total carbon export. Cycles are arranged in order of decreasing vertically integrated chlorophyll concentrations. 'd' denotes deep (100 m) samples; 's' denotes shallow (50 or 60 m samples)

euphausiids, which can form dense aggregations and are hence highly patchy in the CCE (Decima et al. 2010). Thus, it is possible that our broad scale patterns are driven, in part, by the spatial heterogeneity of sampling a euphausiid aggregation. Nevertheless, the general pattern that active transport is a lower proportion of total export in oligotrophic regions remains even if euphausiid active transport were subtracted from the total.

Carbon export in the CCE

The CCE is a dynamic eastern boundary current (EBC) system that typically experiences strong equatorward winds in the spring and summer (Lynn & Simpson 1987, Hickey 1993). These winds drive coastal upwelling and a subsequent spring bloom in the nearshore region, while the offshore region exhibits less variability and is dominated by smaller taxa (Venrick 1998, 2002). As part of this study, we have measured carbon export in water parcels spanning much of the variability in this system, with ^{14}C primary production rates varying from 325 ± 45 mg C m^{-2} d^{-1} on the offshore side of a front to 2314 ± 929 mg C m^{-2} d^{-1} near the springtime Point Conception upwelling source (Landry et al. 2012, Stukel et al. 2012, R. Goericke unpubl. data). While the high productivity regions were dominated by large phytoplankton (Chekalyuk et al. 2012, Taylor et al. 2012), and likely exhibited high rates of new production, they were not characterized by a high e-ratio (ratio of passive export to primary production). In fact, across several studies in the CCE, contemporary measurements of export and primary production suggest a significant negative correlation ($p < 0.05$ for both ^{234}Th-derived and sediment trap-derived measurements; Fig. 12), that is contrary to the traditional paradigm that predicts high e-ratios in productive regions (Laws et al. 2000, Dunne et al. 2005).

The CCE export pattern is driven by the distinct spatial and temporal patterns that are characteristic of an EBC. During spring, an actively growing and grazing community leads to fresh export by contemporaneous autochthonous processes, with recognizable fecal pellets forming a dominant component of both inshore cycles and pigment budgets suggesting that fecal pellet material may account for virtually all sinking flux even offshore. Nevertheless, advection decouples new and export production (Olivieri & Chavez 2000, Plattner et al. 2005, Stukel et al. 2011), leading to lower than expected e-ratios near Point Conception. In autumn, the role of fecal pellets is reduced, and increased C:N ratios of sinking material suggest a more mature community state, with a large proportion of aged detrital particles in the POM pool. In this situation, export is supported by slowly sinking particles generated earlier in the season that have potentially been fragmented and degraded by biological and physical processes. This aged particulate matter may contribute more to vertical flux than the biological processes assessed during short experimental cycles. Such an interpretation is supported by the low spatial variability in passive carbon export at 100 m during P0810 (coefficient of variation was 0.26 during P0810 compared to 0.55 during P0704), despite high mesoscale variability in primary production. Nevertheless, without measurements of particle sinking velocities, it is impossible to determine whether aged particles were sinking slowly, or

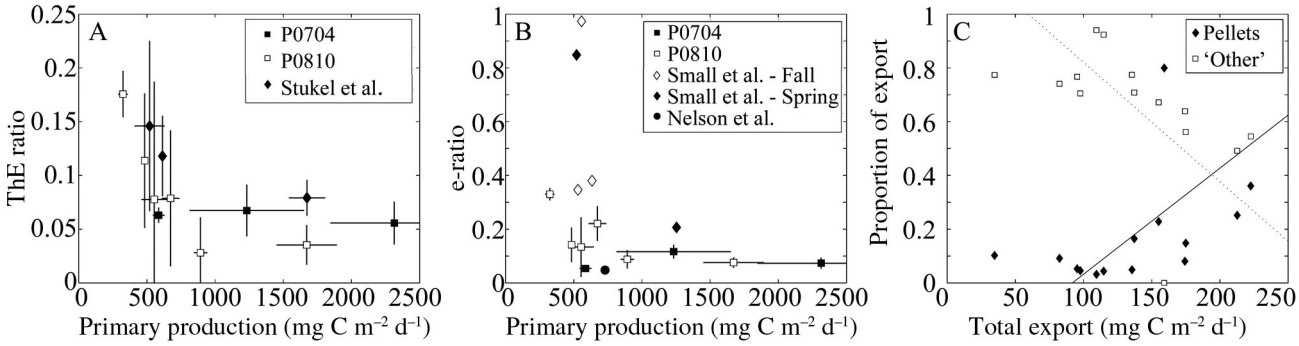

Fig. 12. Passive carbon export in the California Current Ecosystem. (A) ThE ratio (ratio of ^{234}Th-derived organic carbon export to ^{14}C primary production, ^{14}C-PP) as a function of ^{14}C-PP. Squares: this study; diamonds: Stukel et al. (2011). (B) e-ratio (ratio of sediment trap-derived organic carbon export to ^{14}C-PP) versus ^{14}C-PP. Squares: this study; diamonds: Small et al. (1989); circle: Nelson et al. (1987), (other studies conducted in the Santa Monica Basin). In panels (A) and (B), open symbols are spring, filled symbols are October, and error bars (when present) are standard error. ThE and e-ratio are computed with 100 m export for all studies. (C) Proportion of total export (active + passive flux) accounted for by fecal pellets (filled diamonds) and 'other' sinking material (open squares), which is unrecognizable material likely comprised of marine snow aggregates and degraded fecal material. *X*-axis is total flux. Solid line is the model II regression: pellet proportion = 0.0039 × total export − 0.36. Dashed line is the model II regression: 'other' proportion = −0.0044 × total export + 1.26. Spearman's rank correlation found both proportions to be related to total export ($p < 0.05$)

whether a small fraction of suspended particles was continually being scavenged by sinking aggregates.

Another striking result of our study is the relative constancy of 'other' sinking material—unrecognizable material that was likely comprised of a mixture of marine snow aggregates and degraded fecal pellets (Fig. 11). While marine snow contributed a relatively constant flux throughout the region (particularly in the fall), its relative contribution to the biological pump decreased during higher export conditions when fecal pellets were increasingly important (Fig. 12c). This result makes sense if we consider a 2-component sinking detritus pool, comprised of rapidly sinking fecal pellets that are tightly coupled to autochthonous grazing processes and slowly sinking marine snow particles that can be advected greater distances and re-worked by grazers and microbes prior to export. This dichotomy highlights the problem of treating sinking detritus as a static and homogeneous class of particles. Determining the relative contributions of rapidly and slowly sinking material to total passive export is crucial for constraining the remineralization length scale of carbon in the ocean interior, and consequently the length of time that it is removed from contact with the atmosphere by the biological pump.

Acknowledgements. This study was made possible by the efforts of many collaborators on the CCE LTER Process cruises and the captains, resident technicians and crews of the RVs 'Thompson' and 'Melville'. We are especially grateful to A. Cawood, M. Décima, S. Dovel, R. Goericke, T. Langland, S. Pal, W. Plessinger, J. Powell, J. B. Romagnn, M. Roadman, R. Styles, D. A. A. Taniguchi and A. G. Taylor for help with shipboard sample collections and subsequent sample analyses. This work was supported by National Science Foundation (NSF) funding (OCE 0417616 and 1026607) for the CCE LTER site, and by graduate research fellowships (NSF and NASA Earth and Space Science) to M.S.

LITERATURE CITED

Al-Mutairi H, Landry MR (2001) Active export of carbon and nitrogen at Station ALOHA by diel migrant zooplankton. Deep-Sea Res II 48:2083–2103

Alldredge AL, Gotschalk CC (1989) Direct observations of the mass flocculation of diatom blooms: characteristics, settling velocities and formation of diatom aggregates. Deep-Sea Res 36:159–171

Armstrong RA, Lee C, Hedges JI, Honjo S, Wakeham SG (2001) A new, mechanistic model for organic carbon fluxes in the ocean based on the quantitative association of POC with ballast minerals. Deep-Sea Res II 49: 219–236

Benitez-Nelson C, Buesseler KO, Karl DM, Andrews J (2001a) A time-series study of particulate matter export in the North Pacific Subtropical Gyre based on ^{234}Th: ^{238}U disequilibrium. Deep-Sea Res I 48:2595–2611

Benitez-Nelson CR, Buesseler KO, van der Loeff MR, Andrews J, Ball L, Crossin G, Charette MA (2001b) Testing a new small-volume technique for determining ^{234}Th in seawater. J Radioanal Nucl Chem 248:795–799

Brinton E (1967) Vertical migration and avoidance capability of euphausiids in California Current. Limnol Oceanogr 12:451–483

Buesseler KO, Benitez-Nelson C, van der Loeff MR, Andrews J, Ball L, Crossin G, Charette MA (2001) An

intercomparison of small- and large-volume techniques for thorium-234 in seawater. Mar Chem 74:15–28

Buesseler KO, Benitez-Nelson CR, Moran SB, Burd A and others (2006) An assessment of particulate organic carbon to thorium-234 ratios in the ocean and their impact on the application of ^{234}Th as a POC flux proxy. Mar Chem 100:213–233

Buesseler KO, Antia AN, Chen M, Fowler SW and others (2007) An assessment of the use of sediment traps for estimating upper ocean particle fluxes. J Mar Res 65: 345–416

Buitenhuis E, Le Quere C, Aumont O, Beaugrand G and others (2006) Biogeochemical fluxes through mesozooplankton. Global Biogeochem Cycles 20, GB2003, doi: 10.1029/2005GB002511

Burd AB, Hansell DA, Steinberg DK, Anderson TR and others (2010) Assessing the apparent imbalance between geochemical and biochemical indicators of meso- and bathypelagic biological activity: What the @$#! is wrong with present calculations of carbon budgets? Deep-Sea Res II 57:1557–1571

Chekalyuk AM, Landry MR, Goericke R, Taylor AG, Hafez MA (2012) Laser fluorescence analysis of phytoplankton across a frontal zone in the California Current ecosystem. J Plankton Res 34:761–777

Conover RJ (1966) Assimilation of organic matter by zooplankton. Limnol Oceanogr 11:338–345

Conover RJ, Durvasula R, Roy S, Wang R (1986) Probable loss of chlorophyll-derived pigments during passage through the gut of zooplankton, and some of the consequences. Limnol Oceanogr 31:878–887

Dam HG, Peterson WT (1988) The effect of temperature on the gut clearance rate-constant of planktonic copepods. J Exp Mar Biol Ecol 123:1–14

Decima M, Ohman MD, De Robertis A (2010) Body size dependence of euphausiid spatial patchiness. Limnol Oceanogr 55:777–788

Downs JN, Lorenzen CJ (1985) Carbon:pheopigment ratios of zooplankton fecal pellets as an index of herbivorous feeding. Limnol Oceanogr 30:1024–1036

Ducklow HW, Steinberg DK, Buesseler KO (2001) Upper ocean carbon export and the biological pump. Oceanography 14:50–58

Dunne JP, Armstrong RA, Gnanadesikan A, Sarmiento JL (2005) Empirical and mechanistic models for the particle export ratio. Global Biogeochem Cycles 19, GB4026, doi: 10.1029/2004GB002390

Durbin EG, Campbell RG (2007) Reassessment of the gut pigment method for estimating *in situ* zooplankton ingestion. Mar Ecol Prog Ser 331:305–307

Goericke R (2002) Top-down control of phytoplankton biomass and community structure in the monsoonal Arabian Sea. Limnol Oceanogr 47:1307–1323

Goericke R, Strom SL, Bell RA (2000) Distribution and sources of cyclic pheophorbides in the marine environment. Limnol Oceanogr 45:200–211

Gorsky G, Ohman MD, Picheral M, Gasparini S and others (2010) Digital zooplankton image analysis using the ZooScan integrated system. J Plankton Res 32: 285–303

Gowing MM, Silver MW (1985) Minipellets: a new and abundant size class of marine fecal pellets. J Mar Res 43: 395–418

Gowing MM, Wishner KF (1986) Trophic relationships of deep-sea calanoid copepods from the benthic boundary layer of the Santa Catalina Basin, California. Deep-Sea Res 33:939–961

Gowing MM, Garrison DL, Kunze HB, Winchell CJ (2001) Biological components of Ross Sea short-term particle fluxes in the austral summer of 1995-1996. Deep-Sea Res I 48:2645–2671

Hickey BM (1993) Physical oceanography. In: Dailey MD, Reish DJ, Anderson JW (eds) Ecology of the Southern California Bight: a synthesis and interpretation. University of California Press, Berkeley, CA, p 19–70

Ikeda T (1985) Metabolic rates of epipelagic marine zooplankton as a function of body mass and temperature. Mar Biol 85:1–11

Ikeda T, Kanno Y, Ozaki K, Shinada A (2001) Metabolic rates of epipelagic marine copepods as a function of body mass and temperature. Mar Biol 139:587–596

Jackson GA, Waite AM, Boyd PW (2005) Role of algal aggregation in vertical carbon export during SOIREE and in other low biomass environments. Geophys Res Lett 32, L13607, doi:10.1029/2005GL023180

Kiorboe T, Sabatini M (1995) Scaling of fecundity, growth and development in marine planktonic copepods. Mar Ecol Prog Ser 120:285–298

Knauer GA, Martin JH, Bruland KW (1979) Fluxes of particulate carbon, nitrogen, and phosphorus in the upper water column of the Northeast Pacific. Deep-Sea Res 26:97–108

Knauer GA, Karl DM, Martin JH, Hunter CN (1984) *In situ* effects of selected preservatives on total carbon, nitrogen and metals collected in sediment traps. J Mar Res 42:445–462

Landry MR, Lorenzen CJ, Peterson WK (1994) Mesozooplankton grazing in the Southern California Bight. II. Grazing impact and particulate flux. Mar Ecol Prog Ser 115:73–85

Landry MR, Al-Mutairi H, Selph KE, Christensen S, Nunnery S (2001) Seasonal patterns of mesozooplankton abundance and biomass at Station ALOHA. Deep-Sea Res II 48:2037–2061

Landry MR, Ohman MD, Goericke R, Stukel MR, Tsyrklevich K (2009) Lagrangian studies of phytoplankton growth and grazing relationships in a coastal upwelling ecosystem off Southern California. Prog Oceanogr 83:208–216

Landry MR, Ohman MD, Goericke R, Stukel MR, Barbeau KA, Bundy R, Kahru M (2012) Pelagic community responses to a deep-water front in the California Current Ecosystem: overview of the A-Front Study. J Plankton Res 34:739–748

Lavaniegos BE, Ohman MD (2007) Coherence of long-term variations of zooplankton in two sectors of the California Current System. Prog Oceanogr 75:42–69

Laws EA, Falkowski PG, Smith WO, Ducklow H, McCarthy JJ (2000) Temperature effects on export production in the open ocean. Global Biogeochem Cycles 14:1231–1246

Longhurst AR, Bedo AW, Harrison WG, Head EJH, Sameoto DD (1990) Vertical flux of respiratory carbon by oceanic diel migrant biota. Deep-Sea Res 37:685–694

Lynn RJ, Simpson JJ (1987) The California Current System: the seasonal variability of its physical characteristics. J Geophys Res 92:12947–12966

Mauchline J (1998) Introduction. In: Blaxter JHS, Southward AJ, Tyler PA (eds) Advances in marine biology, Vol 33: the biology of calanoid copepods. Academic Press, San Diego, CA, p 1–13

Nelson JR, Beers JR, Eppley RW, Jackson GA, McCarthy JJ, Soutar A (1987) A particle flux study in the Santa Monica-San Pedro Basin off Los Angeles: particle flux, primary production, and transmissometer survey. Cont Shelf Res 7:307–328

Ohman MD, Powell JR, Picheral M, Jensen DW (2012) Mesozooplankton and particulate matter responses to a deep-water frontal system in the southern California Current System. J Plankton Res 34:815–827

Olivieri RA, Chavez FP (2000) A model of plankton dynamics for the coastal upwelling system of Monterey Bay, California. Deep-Sea Res II 47:1077–1106

Olli K, Wassmann P, Reigstad M, Ratkova TN and others (2007) The fate of production in the central Arctic Ocean - Top-down regulation by zooplankton expatriates? Prog Oceanogr 72:84–113

Owens SA, Buesseler KO, Sims KWW (2011) Re-evaluating the ^{238}U-salinity relationship in seawater: implications for the ^{238}U-^{234}Th disequilibrium method. Mar Chem 127:31–39

Penry DL, Frost BW (1991) Chlorophyll *a* degradation by *Calanus pacificus*: dependence on ingestion rate and digestive acclimation to food resources. Limnol Oceanogr 36:147–159

Pike SM, Buesseler KO, Andrews J, Savoye N (2005) Quantification of ^{234}Th recovery in small volume sea water samples by inductively coupled plasma-mass spectrometry. J Radioanal Nucl Chem 263:355–360

Plattner GK, Gruber N, Frenzel H, McWilliams JC (2005) Decoupling marine export production from new production. Geophys Res Lett, 32, L11612, doi:10.1029/2005GL022660

Ricker WE (1973) Linear regressions in fishery research. J Fish Res Board Can 30:409–434

Rykaczewski RR, Checkley DM (2008) Influence of ocean winds on the pelagic ecosystem in upwelling regions. Proc Natl Acad Sci USA 105:1965–1970

Savoye N, Benitez-Nelson C, Burd AB, Cochran JK and others (2006) ^{234}Th sorption and export models in the water column: a review. Mar Chem 100:234–249

Small LF, Ellis SG (1992) Fecal carbon production by zooplankton in Santa-Monica Basin: the effects of body size and carnivorous feeding. Prog Oceanogr 30:197–221

Small LF, Landry MR, Eppley RW, Azam F, Carlucci AF (1989) Role of plankton in the carbon and nitrogen budgets of Santa Monica Basin, California. Mar Ecol Prog Ser 56:57–74

Steinberg DK, Carlson CA, Bates NR, Goldthwait SA, Madin LP, Michaels AF (2000) Zooplankton vertical migration and the active transport of dissolved organic and inorganic carbon in the Sargasso Sea. Deep-Sea Res I 47: 137–158

Strickland JD, Parsons TR (1972) A practical handbook of seawater analysis, 2nd edn. Bull Fish Res Board Can 167:1–310

Stukel MR, Landry MR, Benitez-Nelson CR, Goericke R (2011) Trophic cycling and carbon export relationships in the California Current Ecosystem. Limnol Oceanogr 56:1866–1878

Stukel MR, Landry MR, Ohman MD, Goericke R, Samo T, Benitez-Nelson CR (2012) Do inverse ecosystem models accurately reconstruct plankton trophic flows? Comparing two solution methods using field data from the California Current. J Mar Syst 91:20–33

Sybrandy AL, Niiler PP (1992) WOCE/TOGA Lagrangian drifter construction manual. SIO Ref 91/6, WOCE Report No. 63. Scripps Institute of Oceanography, La Jolla, CA

Takahashi K, Kuwata A, Sugisaki H, Uchikawa K, Saito H (2009) Downward carbon transport by diel vertical migration of the copepods *Metridia pacifica* and *Metridia okhotensis* in the Oyashio region of the western subarctic Pacific Ocean. Deep-Sea Res I 56:1777–1791

Taylor AG, Goericke R, Landry MR, Selph KE, Wick DA, Roadman MJ (2012) Sharp gradients in phytoplankton community structure across a frontal zone in the California Current Ecosystem. J Plankton Res 34:778–789

Turner JT (2002) Zooplankton fecal pellets, marine snow and sinking phytoplankton blooms. Aquat Microb Ecol 27:57–102

Venrick EL (1998) Spring in the California current: the distribution of phytoplankton species, April 1993 and April 1995. Mar Ecol Prog Ser 167:73–88

Venrick EL (2002) Floral patterns in the California Current System off southern California: 1990-1996. J Mar Res 60:171–189

Wilson SE, Steinberg DK, Buesseler KO (2008) Changes in fecal pellet characteristics with depth as indicators of zooplankton repackaging of particles in the mesopelagic zone of the subtropical and subarctic North Pacific Ocean. Deep-Sea Res II 55:1636–1647

Wilson SE, Steinberg DK, Chu FLE, Bishop JKB (2010) Feeding ecology of mesopelagic zooplankton of the subtropical and subarctic North Pacific Ocean determined with fatty acid biomarkers. Deep-Sea Res I 57:1278–1294

Editorial responsibility: Antonio Bode, A Coruña, Spain

Submitted: April 3, 2013; Accepted: June 20, 2013
Proofs received from author(s): September 11, 2013